Developmental Biology xxx (xxxx) xxx

Contents lists available at ScienceDirect

Developmental Biology

journal homepage: www.elsevier.com/locate/developmentalbiology

Effector gene expression underlying neuron subtype-specific traits in the Motor Ganglion of Ciona

Susanne Gibboney [1], Jameson Orvis [1], Kwantae Kim, Christopher J. Johnson, Paula Martinez-Feduchi, Elijah K. Lowe, Sarthak Sharma, Alberto Stolfi [*]

School of Biological Sciences, Georgia Institute of Technology, Atlanta, GA, 30332, USA

A B S T R A C T

The central nervous system of the *Ciona* larva contains only 177 neurons. The precise regulation of neuron subtype-specific morphogenesis and differentiation observed during the formation of this minimal connectome offers a unique opportunity to dissect gene regulatory networks underlying chordate neurodevelopment. Here we compare the transcriptomes of two very distinct neuron types in the hindbrain/spinal cord homolog of *Ciona,* the Motor Ganglion (MG): the Descending decussating neuron (ddN, proposed homolog of Mauthner Cells in vertebrates) and the MG Interneuron 2 (MGIN2). Both types are invariantly represented by a single bilaterally symmetric left/right pair of cells in every larva. Supernumerary ddNs and MGIN2s were generated in synchronized embryos and isolated by fluorescence-activated cell sorting for transcriptome profiling. Differential gene expression analysis revealed ddN- and MGIN2-specific enrichment of a wide range of genes, including many encoding potential "effectors" of subtype-specific morphological and functional traits. More specifically, we identified the upregulation of centrosome-associated, microtubule-stabilizing/bundling proteins and extracellular guidance cues part of a single intrinsic regulatory program that might underlie the unique polarization of the ddNs, the only descending MG neurons that cross the midline. Consistent with our predictions, CRISPR/Cas9-mediated, tissue-specific elimination of two such candidate effectors, Efcab6-related and Netrin1, impaired ddN polarized axon outgrowth across the midline.

1. Introduction

Genetic information is a major determinant of the morphological and physiological properties of individual neurons, as well as the connectivity and function of a nervous system (Baker et al., 2001; Bargmann, 1993; Manoli et al., 2006). Although these can be influenced by external cues and activity-dependent mechanisms (Thompson et al., 2017; Zhang and Poo, 2001), the clearest evidence for genetic determination of neurodevelopment comes from the stereotyped neural circuits that underlie innate behaviors (Kim and Emmons, 2017; Yamamoto and Koganezawa, 2013), or behavioral phenotypes caused by genetic mutations that result in changes to neuronal cell biology or connectivity (Branicky et al., 2014; White et al., 1992). Although a major focus of modern neuroscience is to dissect behavior at the level of individual genes, neurons, and specific synaptic connections (Luo et al., 2008), we have yet to decipher even the simplest nervous systems. Part of this difficulty stems from the fact that few organisms studied so far have proven tractable enough for the simultaneous investigation of gene function, neuronal activity, circuit connectivity and behavior.

The first synaptic connectivity network, or "connectome" (Sporns et al., 2005) to be fully mapped was that of *Caenorhabditis elegans*, a nematode that has only 302 neurons (White et al., 1986). Also a genetic and developmental model organism, *C. elegans* has delivered many key neurobiology breakthroughs, many of which were prompted by specific insights gleaned from the connectome (Chalfie et al., 1985; Jang et al., 2012). A second connectome, that of the larva of the tunicate *Ciona intestinalis,* was recently completed (Ryan et al., 2016, 2017, 2018). Vertebrates are the sister group to the tunicates within the chordate phylum (Delsuc et al., 2006), and this close genetic relationship has prompted the study of conserved, chordate-specific mechanisms of neurodevelopment in *Ciona* (Nishino, 2018). The central nervous system (CNS) of the *Ciona intestinalis* larva has only 177 neurons (Ryan and Meinertzhagen, 2019), making it the smallest described in any animal. This minimal, but comprehensive, connectome has neatly dovetailed with cell lineage and gene regulatory network studies performed on the closely related *Ciona robusta* (Cole and Meinertzhagen, 2004; Horie et al., 2018b; Ikuta and Saiga, 2007; Imai et al., 2009; Nicol and Meinertzhagen, 1988a, b; Sharma et al., 2019). The previously cryptic *C. robusta* was referred to as "*C. intestinalis*" in past studies, but recent evidence suggests splitting the two into distinct species (Pennati et al., 2015). However, the species' embryonic cell lineages appear identical, and all the neurons identified in *C. robusta* have been identified in the *C. intestinalis*

* Corresponding author.
E-mail address: alberto.stolfi@biosci.gatech.edu (A. Stolfi).
[1] These authors contributed equally.

https://doi.org/10.1016/j.ydbio.2019.10.012
Received 25 July 2019; Received in revised form 11 October 2019; Accepted 16 October 2019
Available online xxxx
0012-1606/

connectome (Ryan et al., 2016), suggesting a high degree of conservation of the CNS in the *Ciona* species complex (referred to as simply "*Ciona*" from now on).

Within this CNS, the development of Motor Ganglion (MG) has been studied in greatest detail. Situated at the base of the tail, just dorsal to the notochord, the neurons of the MG form a simple central pattern that drives the swimming behaviors of the larva (Nishino et al., 2010)(Fig. 1A). Of these, a core of only 7 bilaterally symmetric left/right pairs of neurons from the majority of the synaptic connectivity of the MG (Ryan et al., 2016)(Fig. 1B), and can all be traced to the A7.8 pair of blastomeres of the 64-cell stage embryo (Cole and Meinertzhagen, 2004; Navarrete and Levine, 2016)(Fig. 1C). We refer to these as the "core" MG, as additional cells traditionally assigned to the MG have either been shown to be quite removed from the motor network, e.g. AMG neurons, which serve as peripheral nervous system relay neurons (Ryan et al., 2018), or have yet to be visualized by light microscopy, e.g. Motor Neurons 3 through 5 and MG Interneuron 3 (Ryan et al., 2016).

Within the core MG, each neuron is uniquely delineated by its invariant lineage, molecular profile, morphology, and synaptic connectivity (Cole and Meinertzhagen, 2004; Ryan et al., 2016, 2017; Stolfi and Levine, 2011). Here we focus on the comparison between two very different MG interneuron types: the descending decussating neuron (ddN) and MG Interneuron 2 (MGIN2). As their name implies, ddNs are the only neurons whose axons cross the midline before descending towards the tail (Fig. 1D)(Stolfi and Levine, 2011; Takamura et al., 2010). They receive synaptic inputs from peripheral nervous system (PNS) relay neurons and in turn synapse onto other MG neurons, each in particular forming synapses with their respective contralateral Motor Neuron 2 (MN2)(Ryan et al., 2017). The development and synaptic connectivity of the ddNs support homology with the Mauthner cells (M-cells) of the hindbrain of various fish and amphibian species. M-cells initiate the startle reflex during swimming, suggesting the ddNs could be mediating similar unilateral tail muscle flexions ("flicks") in tunicates, in response to mechanosensory stimuli (Ryan et al., 2017). On the other hand, MGIN2s (Fig. 1E) are ipsilaterally-projecting descending interneurons whose most salient morphological trait is their extensive dendritic arborization (Stolfi and Levine, 2011). Like the ddNs, they also form conspicuous synapses with MN2s (Ryan et al., 2016), but receive synaptic inputs mainly from photoreceptor relay neurons and other interneurons of the brain, where the larval light- and gravity-sensing organs are located. Thus, these two MG neurons subtypes might modulate asymmetric swimming behaviors in response to sensory cues processed by distinct thigmotactic (ddNs) and phototactic/geotactic (MGIN2s) pathways (Kourakis et al., 2019; Rudolf et al., 2019; Salas et al., 2018).

Recent advances in single-cell RNAseq have allowed for identification of rare cell types in the Ciona nervous system (Cao et al., 2019; Horie et al., 2018b; Sharma et al., 2019), but the transcriptional profiles of ddNs and MGIN2s during their differentiation remains elusive. Here we use previously validated genetic tools to convert a majority of the Motor Ganglion to ectopic ddNs or MGIN2s, and isolate and profile these neurons at a time when their differentiation and morphogenesis is occurring (Stolfi and Levine, 2011; Stolfi et al., 2011). By analyzing and comparing the transcriptomes of isolated ddNs and MGIN2s, we identified differentially-expressed transcripts enriched in either neuron type and validated the ddN- or MGIN2-specific expression of several genes by mRNA *in situ* hybridization. We hypothesize that many of the genes thus identified are rate-limiting effectors of their unique morphological and physiological characteristics. More specifically, we identify centrosomal

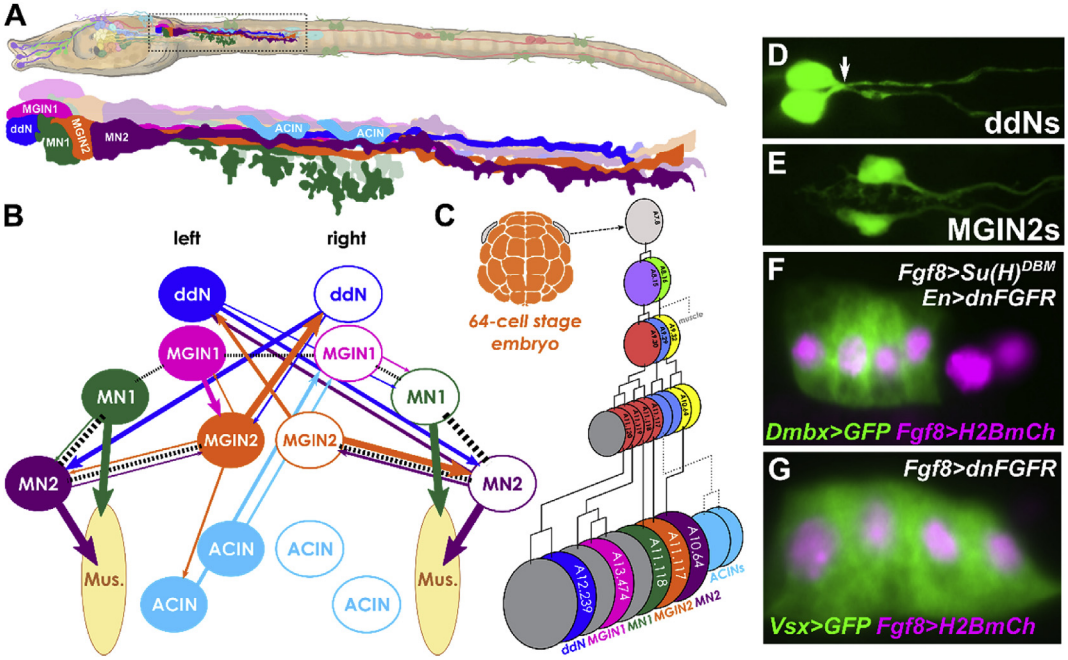

Fig. 1. Neuronal subtypes in the Motor Ganglion of Ciona. **A)** Diagram of a *Ciona* larva, with Motor Ganglion (MG) highlighted and magnified in inset. MG neuron morphologies are drawn according to Ryan and Meinertzhagen (2019). Larva illustration by Lindsey Leigh. **B)** Diagram of core MG connectome, adapted from Ryan et al. (2016). Colored arrows indicate major chemical synapses, dashed lines indicate major gap junctions (electrical synapses). Thickness of lines is proportional to cumulative depth of synaptic contact, except for neuromuscular synapses. Only synaptic connections shown are chemical synapses of cumulative depth >1 μm, and gap junctions of cumulative depth >6 μm. ACIN left/right symmetry is portrayed even though original connectome was missing a second ACIN on right side. ddN: descending decussating neuron, MGIN1: MG interneuron 1, MGIN2: MG interneuron 2, MN1: motor neuron 1, MN2: motor neuron 2, ACIN: ascending contralateral inhibitory neuron, Mus.: muscles. **C)** Cell lineage diagram of core MG neurons inferred from Cole and Meinertzhagen (2004) and Stolfi and Levine (2011), updated by results from Navarrete and Levine (2016) showing A10.64 identity of MN2, and from Nishitsuji et al. (2012) showing descent of ACINs from A9.29 (Cole and Meinertzhagen, 2004; Navarrete and Levine, 2016; Nishitsuji et al., 2012). Unresolved cell divisions in ACIN lineage indicated by dashed lines. **D)** ddN pair labeled with *Dmbx* reporter construct, arrow indicating axons crossing the midline. **E)** MGIN2 pair labeled with *Pitx* reporter construct. **F)** Supernumerary ddNs generated by early Notch/late FGF inhibition. This condition was used to isolate ddNs by FACS. **G)** Supernumerary MGIN2s generated by early FGF inhibition, condition used to isolate MGIN2s by FACS. Panels D, E, and G adapted from Stolfi and Levine (2011). Panel F adapted from Stolfi et al. (2011).

microtubule-stabilizing proteins and extracellular guidance cues as potential effectors, all expressed by the ddNs themselves, that together might direct the unique mode of polarization and axon outgrowth that we document in the ddNs.

2. Materials and methods

2.1. Ciona robusta collection and handling

Adult *Ciona robusta* (*intestinalis* Type A) were collected from Pillar Point Marina (Half Moon Bay, CA) or San Diego, CA (M-REP). Dechorionated embryos were obtained and electroporated as previously described (Christiaen et al., 2009a, b). Sequences of plasmids and *in situ* hybridization probe templates not previously published can be found in the **Supplemental Sequences** file. Fluorescent, whole-mount *in situ* hybridization and immunostaining were carried out as previously described (Beh et al., 2007; Ikuta and Saiga, 2007; Stolfi et al., 2011). Images were captured using Nikon, Leica, or Zeiss epifluorescence compound microscopes.

2.2. Whole embryo dissociation for FACS

Embryos were electroporated with the following combinations of plasmids, previously published and described (Stolfi et al., 2011). A mix of 60 μg *Fgf8/17/18 > Su(H)^{DBM}* + 60 μg *Engrailed > dnFGFR* + 61 μg *Dmbx > Unc-76::GFP* + 58 μg *Twist-related.b > RFP* was to generate and isolate ectopic ddNs ("ddN" condition). Briefly, *Fgf8/17/18 > Su(H)^{DBM}* suppresses Notch signaling in the A9.30 lineage, resulting in duplication of the A11.120 cell, while *Engrailed > dnFGFR* suppresses FGF signaling in the anterior A9.30 lineage (A11.119 and A11.120), thus converting their progeny to ddNs (Stolfi et al., 2011). A mix of 60 μg *Fgf8/17/18 > dnFGFR* + 60 μg *En > lacZ* + 61 μg *Vsx > Unc-76::GFP* + 58 μg *Twist-related.b > RFP* was used to generate and isolate ectopic MGIN2s ("IN2" condition) Briefly, *Fgf8/17/18 > dnFGFR* suppresses FGF signaling early in the A9.30 progenitor, converting the whole lineage into 4 MGIN2 cells on either side of the embryo (Stolfi and Levine, 2011; Stolfi et al., 2011). *En > lacZ* is a neutral construct used to normalize the total amount of plasmid DNA electroporated when compared to the ddN condition. Unc-76 tags (Dynes and Ngai, 1998; Stolfi and Levine, 2011) are used to label the entire cytoplasm, as opposed to untagged GFP, which tend to accumulate in the nucleus and is not efficiently transported into the axons. Additional unelectroporated embryos were raised in parallel, for sorted, unlabeled cells from whole embryos ("Whole" condition) Embryos were grown to 15.5 h post-fertilization (hpf) at 16 °C (Hotta Stage 23)(Hotta et al., 2007a) and dissociated in trypsin and Ca++/Mg + -free artificial sea water as previously described (Wang et al., 2018). We chose to dissociate right before ddN polarity inversion occurs (see Fig. 5), to maximize chance of observing upregulation of polarization effector genes. All plasmid amounts are given in μg per 700 μl of total electroporation solution.

2.3. Fluorescence-activated cell sorting (FACS) and microarray profiling

FACS was performed on a Coulter EPICS Elite ESP sorter (Coulter Inc.), as previously described (Christiaen et al., 2008), with GFP + cells selected and RFP + cells counterselected. "Whole embryo" cells corresponding to cells dissociated from whole unelectroporated embryos were isolated in parallel. RNA extraction was performed using RNAqueous-micro kit (ThermoFisher) as per manufacturer protocol and analyzed by BioAnalyzer (Agilent). Total RNA amounts calculated to correspond to 1364 GFP + cells was used to prepare each cDNA sample, normalized based on the GFP + sample that yielded the lowest RNA concentration. Due to even lower RNA concentrations for GFP- "whole embryo" sorted cells, 833 cells were used for replicates 1 and 2, and 2083 for replicate 3, maxing out the volume of RNA solution allowed for cDNA synthesis. See Supplemental Table 1 for detailed information about each sample used for cDNA synthesis. We used the Ovation Pico WTA System (NuGen) and the Encore Biotin Module (NuGen) to prepare cDNAs and target probes for microrarray, following the manufacturer's instructions and as previously described (Razy-Krajka et al., 2014). Microarray hybridization, washing, staining, and scanning were performed on a custom Affymetrix GeneChip (ArrayExpress accession A-AFFY-106) according to NuGen protocols and as previously described (Christiaen et al., 2008; Razy-Krajka et al., 2014).

Raw expression values (e.g. .CEL files) for each probe over three biological replicates for each condition ("IN2", "ddN", and "Whole") were used to normalize and compute probe set expression estimates using the robust multi-chips analysis (RMA) algorithm (RMAexpress software) (Bolstad et al., 2003; Smyth, 2004). RMA estimates are available at https://osf.io/n7vr2/and Supplemental Table 2. RMA estimates were averaged across replicates and then converted to Log2 and pair-wise fold-change comparisons (LogFC) calculated (e.g. Log2[condition X RMA average] – Log2[condition Y RMA average) and P-values given by 1-tailed type 1 T-test. Probesets were matched to KyotoHoya (KH) gene models (Satou et al., 2008), or prior gene models when KH gene models did not appear to match a probeset sequence. See Supplemental Table 3 for our new annotation of correspondences between probesets and gene models.

2.4. CRISPR/Cas9-mediated mutagenesis

CRISPR/Cas9 was performed as established, using *Foxa.a>Cas9* to drive expression in vegetal hemisphere lineages (A/B)(Di Gregorio et al., 2001), or *Fgf8/17/18 > Cas9* to drive expression in the A9.30 lineage, though it is also active in mesenchyme, tail nerve cord, and tail tip neurons (Imai et al., 2009). Single-chain guide RNAs (sgRNAs) were designed and selected using CRISPOR (Haeussler et al., 2016), and vectors constructed as described (Gandhi et al., 2018). The sgRNA vectors were validated using the peakshift method (Gandhi et al., 2017), so-called due to overlapping "peaks" seen in Sanger sequencing of amplicons from the targeted locus amplified from pooled embryos; the overlapping "peaks" result from a mix of molecules containing indels of different sizes (Hsiau et al., 2019). We also validated sgRNAs by a novel "plasmid cutting assay", using GFP fusions (*Efcab6-r::GFP, Netrin1::GFP*) driven by an *Ebf* driver that drives expression in *Ebf* + neuronal progenitors (Stolfi and Levine, 2011). Efficient sgRNAs will cleave all the GFP fusion-encoding plasmids, resulting in loss of GFP fluorescence. All sgRNA sequences and peakshift primers are in the Supplemental Sequences file. *Efcab6r.157* sgRNA was validated as cutting *Efcab6-related* (Supplemental Fig. 1), and *Netrin1.364* was validated as cutting *Netrin1* (Supplemental Fig. 2). For *Efcab6-related* axon outgrowth assay, we electroporated 30 μg of *Foxa.a>Cas9* 90 μg + *Dmbx > Unc-76::YFP* + 50 μg of *U6>Efcab6r.157*. The "control" for this experiment was identical but using 50 μg *U6>Cesa4.1* (gift from Lionel Christiaen), designed to target *Cellulose synthase,* a gene expressed only in epidermis (Nakashima et al., 2004) and therefore not of predicted functional importance in the vegetal lineages where *Foxa.a>Cas9* was to be expressed. For *Netrin1* axon trajectory assay, we electroporated 70 μg *Fgf8/17/18 > Cas9* + 90 μg *Dmbx > Unc-76::GFP* + 70 μg of *U6>Netrin1.364*. For *Netrin1* polarity assay, we electoporated 70 μg *Fgf8/17/18 > Cas9* + 25 μg *Fgf8/17/18 > Galnact::YFP* + 25 μg *Fgf8/17/18 > H2B::mCherry* + 70 μg *U6>Netrin1.364*. The controls for these experiments were identical but using instead 70 μg of *U6>ControlF + E* plasmid (control "target" sequence that does not exist in *Ciona* genome: gctttgctacgatctacatt)(Stolfi et al., 2014). All plasmid amounts are given in μg per 700 μl of total electroporation solution.

3. Results and discussion

We used fluorescence-activated cell sorting (FACS) to isolate specific MG neuron types from synchronized *Ciona robusta* (*intestinalis Type A*) embryos, allowing us to profile their transcriptomes. We took advantage of different genetic manipulations to convert the majority of MG neurons into

either supernumerary ddNs or supernumerary MGIN2s, which normally arise from a common progenitor at the neurula stage, the A9.30 pair of blastomeres of the neural plate (Fig. 1A)(Stolfi and Levine, 2011). We previously established that irreversibly inhibiting early Notch and late FGF signaling in the anterior cells of the A9.30 lineage converts their progeny into ectopic ddNs, all expressing the ddN marker *Dmbx* (Fig. 1F). In contrast, irreversibly inhibiting early FGF signaling converts the entire A9.30 lineage into ectopic MGIN2s, all expressing the MGIN2 marker *Vsx* (Fig. 1G). To generate ectopic ddNs or MGIN2s for fluorescence-activated cell sorting (FACS)-mediated cell type isolation, we recapitulated these perturbation conditions by co-electroporating synchronized embryos with specific combinations of plasmids (see Materials and methods for details). Ectopic ddNs were then isolated based on *Dmbx > GFP* expression, while ectopic MGIN2s were isolated by *Vsx > GFP* expression. In both conditions, co-electroporation with *Twist-related.b(KH.C5.554)>RFP* (Abitua et al., 2012) was used to counterselect mesenchyme cells potentially contaminating of our otherwise pure populations of MG neuron types. Embryos were dissociated at 15.5 h post-fertilization (hpf) at 16 °C. Control "whole embryo" cells were dissociated from un-electroporated embryos and subjected to FACS without selection. Total RNA was extracted from sorted cells, followed by cDNA synthesis and transcriptome profiling by microarray, in three independent biological replicates for each condition (see Materials and methods for details).

cDNA libraries were hybridized to Custom-designed Affymetrix GeneChip microarrays (ArrayExpress accession A-AFFY-106)(Christiaen et al., 2008) to quantify transcripts in sorted ddN, MGIN2, and mixed whole-embryo cells, and calculate the enrichment or depletion of ~21, 000 individual transcript models in each cell population (Supplemental Table 2). Although the custom-made Affymetrix GeneChip microarrays we used were designed prior to the release of the most recent *C. robusta* genome assembly and associated transcript models (KyotoHoya, or KH)(Satou et al., 2008), we re-linked probesets to KH gene models where possible (see Materials and methods for details). Pairwise comparison of ddN and MGIN2 probeset expression values revealed a list of candidate genes that are differentially up- and/or down-regulated in either MG neuron subtype (Supplemental Table 2).

We detected 982 probesets that were significantly enriched (LogFC> 0.6, $p < 0.05$) in the ddNs vs. the MGIN2s, and 1245 probesets significantly enriched in MGIN2s vs. ddNs (LogFC < -0.6, $p < 0.05$). This is a slight overestimation of enriched *genes,* since many genes appear to be represented by more than one probeset, due to imprecise gene annotation. By perusing previously published expression patterns of some of the top differentially-expressed genes, we deduced that our FACS-isolated MGIN2 population contained contaminating cells that we failed to counterselect. MGIN2s appeared to be contaminated with epidermis midline cells, based on the presence of epidermal midline markers *Dlx.c* and *Klf1/2/4* (Imai et al., 2004) in our top 25 MGIN2-enriched genes. This was likely due to the weak expression of *Vsx > GFP* in the dorsal epidermis midline (Supplemental Fig. 3). This contamination might explain the slightly higher number of genes enriched in the MGIN2 samples. Although *Vsx > GFP* is also expressed in MGIN1 (A13.474 cell)(Stolfi and Levine, 2011), such contamination was not a concern, due to the fact that we previously established that our molecular perturbation (*Fgf8/17/18 > dnFGFR*) converts the whole lineage to MGIN2 neurons, abolishing MGIN1 neurons (Stolfi et al., 2011).

We next selected a subset of the top differentially expressed genes in either MGIN2s (Table 1) or ddNs (Table 2) to validate by whole-mount fluorescent mRNA *in situ* hybridization (ISH). Some genes were selected on the basis of their statistically significant enrichment in either population, or based on their potential interest to us as candidates for follow-up functional studies.

3.1. MGIN2-enriched transcripts

While several ddN-specific markers have been previously described, there are relatively few known markers of MGIN2 other than *Vsx*. Although *Vsx* was indeed the gene that was most enriched in MGIN2s in our dataset (Table 1, Supplemental Table 2), this enrichment could be attributed to expression of the *Vsx > GFP* plasmid used to sort these cells, which contains portions of the *Vsx* coding sequence.

The second-most enriched transcript we identified in MGIN2 was *Chrnb* (LogFC = 3.7), encoding a beta (non-alpha) subunit of the neuronal nicotinic acetylcholine receptor. *Chrnb* was not found in the current KyotoHoya genome assembly, but is represented by previous gene models. We designed an ISH probe based on the *KYOTOGRAIL.2005.771.2.1* gene model, which revealed highly specific expression in differentiating MGIN2s (Fig. 2A). According to the *C. intestinalis* connectome, MGIN2 receives synaptic inputs primarily from Photoreceptor Relay Neurons (prRNs), which in turn receive inputs primarily from Group I photoreceptors (Kourakis et al., 2019; Ryan et al., 2016). Recent experimental evidence suggests that the negative phototactic behavior of *Ciona* larvae is mediated by directional light detected Group I photoreceptors, while Group II photoreceptors mediate a light dimming "shadow response". In the most recent model of the negative phototactic neural circuit, acetylcholine neurotransmission from prRNs onto the MG might provide the synaptic link between visual processing and motor control (Kourakis et al., 2019). Thus, acetylcholine receptors formed in part by Chrnb subunits might be mediating this crucial step in the visuomotor pathway of *Ciona*.

In addition to cholinergic transmission, GABAergic transmission has been proposed to play a minor role in the negative phototactic pathway, and a major role in the shadow response pathway (Brown et al., 2005; Kourakis et al., 2019). We detected enrichment of transcripts from the GABA receptor subunit delta-encoding gene *Gabrd* (*KH.C1.1254,* LogFC = 2.6) in MGIN2, which we confirmed by ISH (Fig. 2B). In the future it will be interesting to ascertain whether this localized expression confirms the requirement of GABAergic neurotransmission in negative phototaxis or whether it implicates a cryptic role for MGIN2 in the shadow response.

In contrast to acetylcholine and GABA, no role for direct glutamate neurotransmission onto the MG has been proposed. However, we identified MGIN2-specific enrichment of transcripts for the NMDA-type ionotropic glutamate receptor-encoding gene *Grin*, which was validated by ISH (*KH.S2302.1*, LogFC = 2.2, Fig. 2C). While most prRNs that provide synaptic input onto MGIN2 are predicted to be cholinergic and/or GABAergic, we detected the presence of putative glutamatergic neurons projecting to and making contact onto MGIN2 in larvae co-electroporated with *Slc17a6/7/8(Vglut)>tagRFP* (Horie et al., 2008; Stolfi et al., 2015a) and *Vsx > GFP* reporter plasmids (Fig. 2D). The identity of these MGIN2-contacting brain neurons remains elusive, but could be Apical Trunk Epidermal Neurons (ATENs)(Imai and Meinertzhagen, 2007). According to the connectome (Ryan et al., 2016), MGIN2 also receives substantial input from other classes of brain neurons, including antenna relay neurons, which presumably relay positional information from the otolith-attached antenna cells, and coronet relay neurons, which presumably relay information of unknown nature from dopaminergic coronet cells (Moret et al., 2005). Larval swimming and attachment are modulated by gravity, which is lost in larvae lacking an otolith (Jiang et al., 2005; Tsuda et al., 2003). Furthermore, the shadow response can be altered by pharmacological treatments predicted to interfere with dopamine that is presumably released by the coronet cells (Razy-Krajka et al., 2012). Therefore, it is possible that *Grin* expression in MGIN2 is necessary for the modulation of swimming behavior by as of yet unidentified glutamatergic neurons.

Other potential effectors of MGIN2 function that we detected as highly enriched in MGIN2 and validated by ISH included *Kcna.a* (*KH.C1.232,* LogFC = 3.1, Fig. 2E), encoding a Shaker-related, voltage-gated potassium channel, closely related to TuKv1 (Ono et al., 1999) from *Halocynthia roretzi,* a distantly related tunicate species. Another candidate was *Protocadherin.e* (*Pcdh.e, KH.C9.518,* LogFC = 2.7, Fig. 2F). Protocadherins play numerous roles in morphogenesis, including being extensively implicated in dendrite morphogenesis and dendritic

Table 1
MGIN2-enriched genes selected for validation by *in situ* hybridization.

Gene name	Gene model ID	LogFC* MGIN2 vs. ddN	p-value	Confirmed by ISH?
Chrnb	KYOTOGRAIL2005.771.2.1	3.7	0.009	YES
Kcna.a	KH.C1.232	3.1	0.002	YES
Slc24a4	KH.L132.15	2.9	0.016	YES**
Protocadherin.e	KH.C9.518	2.7	0.044	YES
Gabr.d	KH.C1.1254	2.6	0.014	YES
Grin	KH.S1211.3	2.2	0.066	YES
Ncs	KH.C1.1067	2.0	0.015	YES**

* for genes represented by more than one probeset, we indicate the highest statistically-significant ($p < 0.05$) LogFC value. LogFC values are inverted relative to Table 1 and Supplemental Table 2, to denote enrichment in MGIN2 vs. ddN.
** *Slc24a4* and *Ncs* were enriched in MGIN2 and MN2 relative to ddN.
Red font highlights either $p > 0.05$, or "NO" *in situ* hybridization validation.

Table 2
ddN-enriched genes selected for validation by *in situ* hybridization.

Gene name	Gene model ID	LogFC* ddN vs. MGIN2	p-value	Confirmed by ISH?
Lhx1/5	KH.L107.7	3.2	0.004	YES
Fam167	KH.C2.629	3.1	0.044	YES
Efcab6-related	KH.C1.1218	2.9	0.033	YES
Mnx	KH.L128.12	2.6	0.031	YES**
Saxo	KH.C10.475	2.6	0.008	YES
Calmodulin1-related	KH.C8.573	2.3	0.064	YES
Nckap5	KH.C9.229	2.2	0.009	YES
Ephrin a.d	KH.C3.716	2.1	0.013	YES**
Fibrillin	KH.C1.184	1.9	0.042	NO
Fibronectin-related	KH.C2.667	1.7	0.036	YES
Pou4	KH.C2.42	1.7	0.005	YES
Myosin10	KYOTOGRAIL2005.152.13.2	1.6	0.010	NO
Scna.a	KH.C9.462	1.6	0.029	YES**
Mpc	KH.C1.85	1.3	0.016	YES
Netrin1	KH.C12.72	1.3	0.052	YES

* for genes represented by more than one probeset, we indicate the highest statistically-significant ($p < 0.05$) LogFC value. Complete dataset available in Supplemental Table 2.
** *Mnx* was enriched in ddN, MN1, and MN2 relative to MGIN2. *Ephrin a.d* and *Scna.a* were enriched in ddN and MN1 relative to MGIN2.
Red font highlights either $p > 0.05$, or "NO" *in situ* hybridization validation.

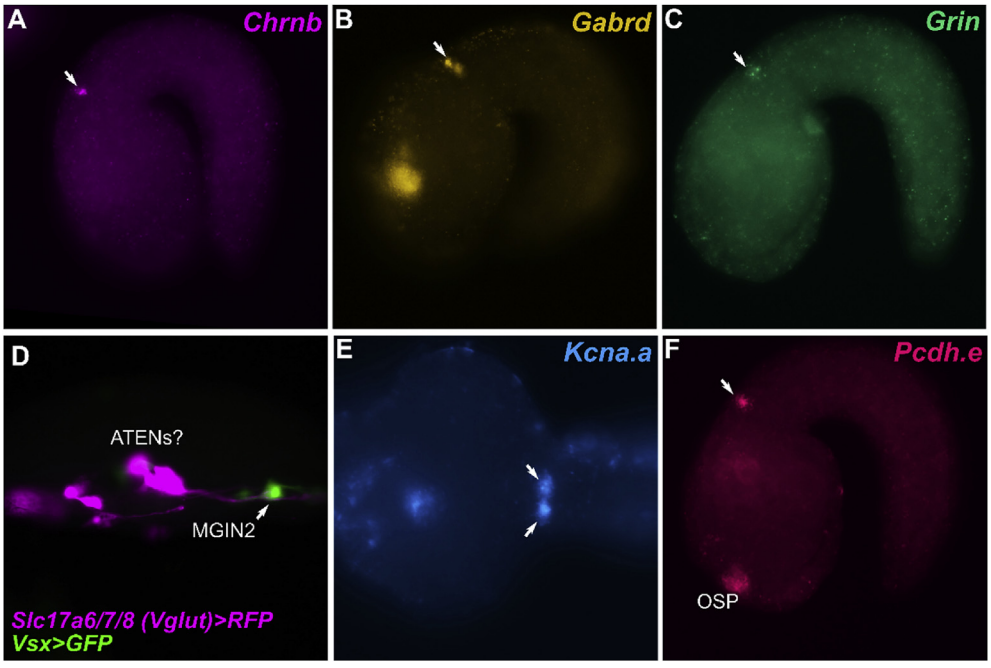

Fig. 2. Candidate effector genes preferentially expressed in MGIN2 vs. ddN. *In situ* hybridization of neurotransmitter receptor subunit-encoding transcripts **A)** *Chrnb (neuronal nicotinic acetylcholine receptor, beta/non-alpha subunit)*, **B)** *Gabrd (GABA receptor subunit delta)*, **C)** *Grin (NMDA-type ionotropic glutamate receptor)*. **D)** Larva electroporated with *Slc17a6/7/8(Vglut)>RFP* (magenta) labeling glutamatergic neurons and *Vsx > GFP* (green) labeling MGIN1 and MGIN2. Axons from unidentified glutamatergic neurons (possibly Apical Trunk Epidermal Neurons, or ATENs) extend and contact MGIN2, suggesting an unknown glutamatergic sensory relay input into the MG via MGIN2. **E)** *In situ* hybridization of transcripts encoding the Shaker-type voltage-gated potassium channel (*Kcna.a*). **F)** *In situ* hybridization of *Protocadherin.e*. OSP: oral siphon primordium. Arrows in all panels indicate MGIN2.

arborization (Keeler et al., 2015). Thus, its specific expression in MGIN2 could be related to its relatively elaborate dendrites, a morphological hallmark of MGIN2 (Stolfi and Levine, 2011)(Fig. 1B).

All the above were confirmed to be expressed in the MGIN2 by two-color double *in situ* hybridization with *Vsx* as the second probe (Supplemental Fig. 4) or immunostaining+*in situ* hybridization in the case of *Kcna.a* (Supplemental Fig. 5). We also found 2 genes that by ISH seemed to be enriched in both MGIN2 and MN2 (Supplemental Fig. 6), but not in other MG neurons: *Slc24a4 (KH.L132.15,* LogFC = 2.9*)* and *Neuronal calcium sensor (Ncs,* also known as *Frequenin, KH.C1.1067,* LogFC = 2.0*)*, further suggesting that many effectors might not be strictly neuron subtype-specific, but that specific combinations of unique and shared effectors may precisely delineate MG neuron functions.

3.2. ddN-enriched regulators

Our basic strategy was validated by the presence of previously characterized ddN markers among top differentially expressed genes. Although *Dmbx* was indeed the most enriched transcript in the ddNs (LogFC = 6.1), this may have been a result of the probeset detecting portions of the *Dmbx > GFP* reporter that was used to select these cells by FACS. In addition to *Dmbx,* known ddN markers *Lhx1/5* (LogFC = 3.2, Fig. 3A), *Pou4* (LogFC = 1.7, Fig. 3B), and *Hox1* (LogFC = 1.6) were among the statistically significant ($p < 0.05$), top 35 genes most enriched in ddNs relative to MGIN2s. These are all transcription factor-encoding genes and have been previously validated by ISH (Imai et al., 2009; Stolfi et al., 2011). We also found that another transcription factor-encoding gene, *Mnx* (Fig. 3C), and an Ephrin signaling molecule-encoding gene, *Ephrin a.d (Efna.d,* KH gene model identifier *KH.C3.716,* Fig. 3D) were also highly enriched in the ddNs relative to MGIN2s (LogFC = 2.6 and 2.1, respectively). Expression of *Mnx* and *Efna.d* had not been previously reported in ddNs, but our ISH validation confirmed their expression in the ddN (Fig. 3C,D). *Mnx* transcripts were also detected in MN1 and MN2, confirming previous ISH (Imai et al., 2009), while *Efna.d* was also expressed in the sister cell of the ddN (A12.240, which does not give rise to a differentiated neuron in the larval stage), and MN1.

Beyond genes encoding transcription factors and signaling molecules, no other potentially ddN-specific transcripts have been previously assayed in detail by ISH. We therefore focused on these, hoping to identify candidate effectors of ddN development and function. For instance, we detected an enrichment for transcripts from the *Sodium voltage-gated channel subunit alpha a* gene *(Scna.a, KH.C9.462,* LogFC = 1.6), encoding a voltage-gated sodium channel orthologous to vertebrate NaV1 channels (Katsuyama et al., 2005; Nishino and Okamura, 2018; Okamura et al., 2005). By ISH, we found that *Scna.a* is upregulated specifically in the ddN and in MN1, but not in MGIN2 nor in any other MG neurons at around stage 23 (~15.5 hpf at 16 °C), when most are differentiating (Fig. 3E). *Ciona* NaV1 (encoded by *Scna.a*) possesses a short, chordate-specific "anchor motif" that in vertebrates is required for dense clustering it the axon initial segment (AIS) through ankyrin-mediated interactions with an actin-spectrin network (Garrido et al., 2003; Hill et al., 2008; Lemaillet et al., 2003). This clustering is crucial for rapid action potential initiation in the proximal axon (Kole et al., 2008). Vertebrate neurons that show dense AIS-specific clustering of NaV1 channels include M-cells and spinal motor neurons (Hill et al., 2008), proposed homologs of ddN and MN1/2, respectively (Ryan et al., 2017). The expression of *Scna.a* in *Ciona* ddN and MN1 suggests that the excitability of these neurons (and ultimately their function) might be similar to those of their vertebrate counterparts, regulated by a conserved, chordate-specific mechanism of subcellular compartmentalization of voltage-gated sodium channels.

3.3. Centrosome-enriched proteins are upregulated in ddNs

Two genes encoding homologs of centrosome-enriched, microtubule-stabilizing proteins were identified among the top ddN-expressed transcripts: *Stabilizer of axonemal microtubules (Saxo, KH.C10.475,* LogFC = 2.6*)* and *Nck-associated protein 5 (Nckap5, KH.C9.229)*. We confirmed the upregulation of both genes in *Ciona* ddNs by ISH (Fig. 4A,B). *Saxo* is the sole *C. robusta* ortholog of human *SAXO1* and *SAXO2,* previously known as *FAM154A and FAM154B* respectively. In humans, SAXO1 was found to bind to centrioles and stabilize microtubules (Dacheux et al., 2015). Similarly, *Nckap5* is an ortholog of the closely related human paralogs *NCKAP5* and *NCKAP5L*. In mammals, *NCKAP5L* encodes Cep169, a centrosome-enriched protein that also stabilizes microtubules (Mori et al., 2015a, 2015b). In our profiling, a single probeset detected enrichment of *Saxo,* but fragmented annotation of earlier versions of the *C. robusta* genome resulted in at least 5 independent probesets that we manually annotated as covering the updated *Nckap5* gene model (*KH.C9.229*). These 5 probesets were all significantly enriched in ddNs relative to MGIN2s (LogFC 1.6-2.2, average 1.8).

In addition to these orthologs of genes encoding previously characterized centrosomal proteins, we also noticed enrichment of *KH.C1.1218* (LogFC = 2.9, Fig. 4C), encoding an EF-hand calcium-binding domain-containing protein (See **Supplemental Sequences**). The predicted protein is weakly similar to human EFCAB6 (also known as DJ-1 Binding Protein, or DJBP) but much more similar to many vertebrate genes annotated as "Efcab6-like". However, *KH.L125.4* (and not *KH.C1.1218)* is the predicted *Ciona* ortholog of human *EFCAB6* according to the inParanoid ortholog prediction program (O'Brien et al., 2005). Alignment and phylogenetic analysis in MAFFT (Katoh et al., 2017) of several related genes suggests KH.C1.1218 closely resembles platypus Efcab6-like (XP_028932998.1), which lacks a clear 1-to-1 ortholog in human but

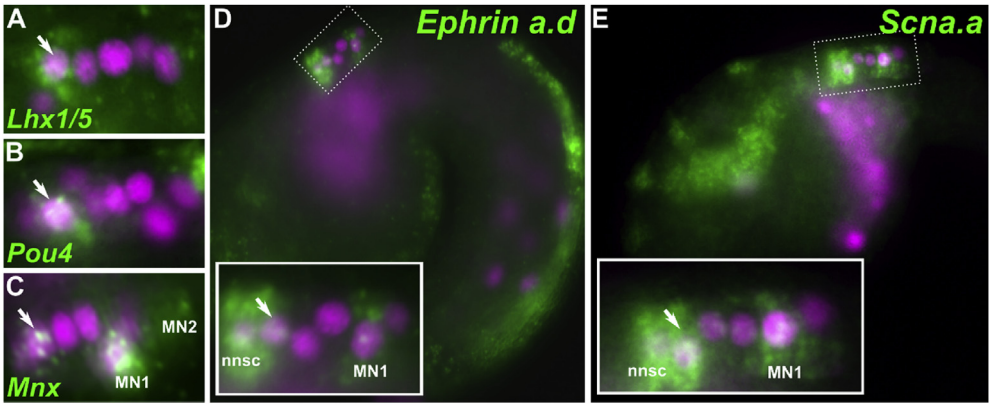

Fig. 3. Genes preferentially expressed in ddN vs. MGIN2. Immunostaining of Beta-galactosidase or H2B::mCherry (magenta) in A9.30 lineage progeny nuclei (*Fgf8/17/18* reporters, which also label mesoderm) coupled to *in situ* hybridization (green) of transcripts encoding transcription factors **A)** *Lhx1/5*, **B)** *Pou4*, **C)** *Mnx*, **D)** signaling molecule *Ephrin a.d,* and **E)** voltage-gated sodium channel subunit *Scna.a*. Arrows indicate ddNs. nnsc: non-neuronal sister cell of ddN (A12.240).

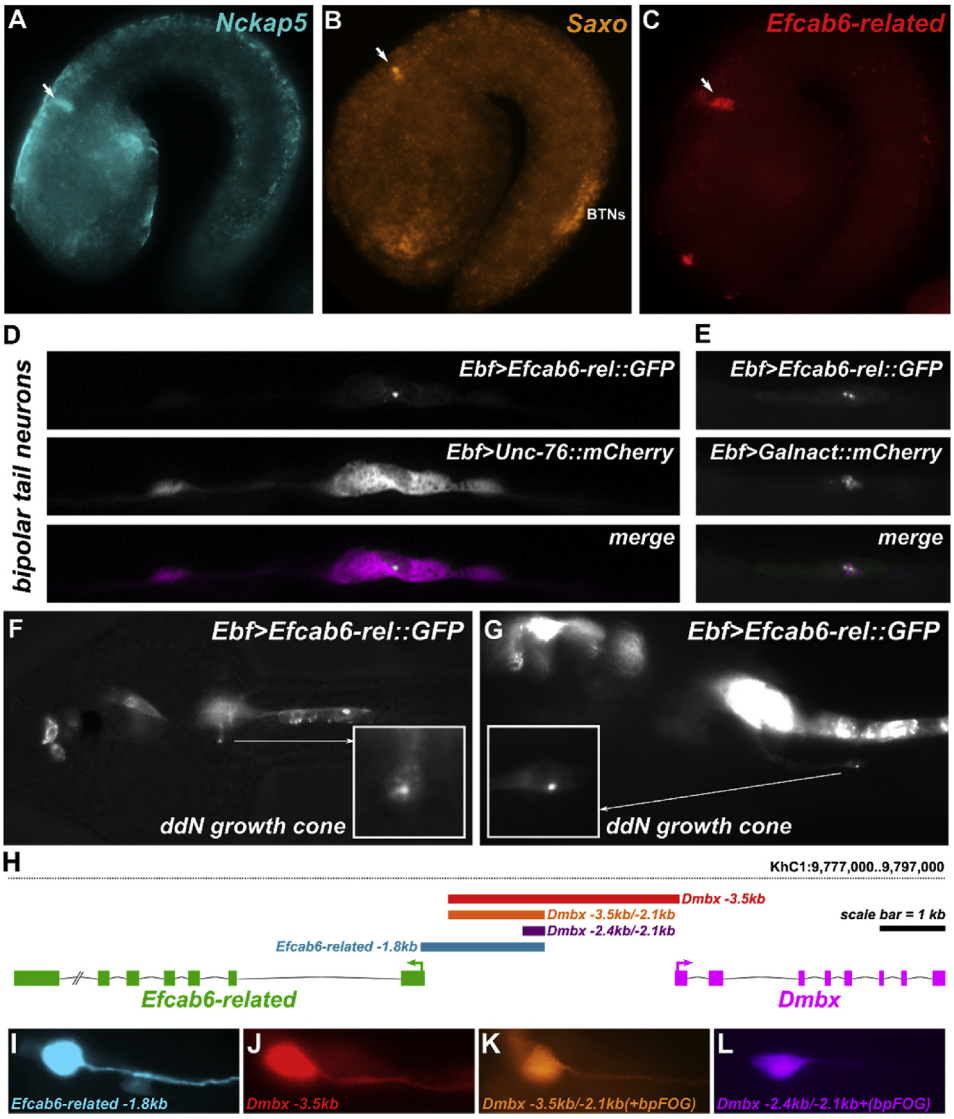

Fig. 4. Genes encoding centrosome-localized microtubule-binding proteins are enriched in ddNs. *In situ* hybridization of **A)** *Nckap5,* **B)** *Saxo,* and **C)** *Efcab6-related.* Arrows indicate ddNs. BTNs: Bipolar Tail Neurons. **D)** Efcab6-related::GFP (driven by *Ebf* promoter) labeling the centrosome in a differentiating Bipolar Tail Neuron. **F)** Co-electroporation of *Ebf > Efcab6-related::GFP* and *Ebf > Galnact::mCherry* reveals association of centrosome with Golgi apparatus in the BTNs, as seen in vertebrate cells. Efcab6-related::GFP labels a small punctum in the axon growth cone of a ddN as it extends across the midline. **G)** Efcab6-related::GFP punctum also in the growth cone of the ddN axon turning and extending posteriorly down the tail. **H)** Diagram of *Efcab6-related* and *Dmbx* loci and shared *cis*-regulatory sequences. **I-L)** Expression of various *Efcab6-related/Dmbx* reporters in the ddN, color coded according to the diagram in panel H.

still clusters with KH.L125.4 and human EFCAB6 (**Supplemental Sequences**). This suggests that the ortholog of *KH.C1.1218* may have been lost in placental mammals. For these reasons, we refer to *KH.C1.1218* as *Efcab6-related,* to indicate a close but unresolved phylogenetic relationship to human *EFCAB6,* as per the tunicate gene nomenclature guidelines (Stolfi et al., 2015b).

In human cells, EFCAB6 can inhibit the transcriptional activity of androgen receptor (Niki et al., 2003) through its association with DJ-1, a regulator of oxidative stress response and mitochondrial function (Canet-Avilés et al., 2004; Wang et al., 2012). A mouse knockout line from the Knock Out Mouse Phenotyping Program (KOMP^2, Jackson Laboratory) for Efcab6 shows inserted reporter gene staining in the developing hindbrain (https://www.mousephenotype.org/data/genes/MGI:1924877), suggesting a potentially conserved role in M-cell/ddN development. Given its seven EF-hand domains, we hypothesized that Efcab6-related might be localized to centrosomes, much like other EF hand-containing, calcium-binding proteins like Centrin or Calmodulin (Ito and Bettencourt-Dias, 2018). Indeed, an Efcab6-related::GFP fusion was specifically localized to the centrosome of the bipolar tail neurons (Stolfi et al., 2015a)(Fig. 4D), co-localizing with the Golgi apparatus (Fig. 4E). In ddNs, we detected a small punctum of Efcab6-related::GFP in the axon growth cone during extension over the midline (Fig. 4F) and later down the tail (Fig. 4G), but we were unable to visualize its localization earlier. These localization patterns hint at previously unrecognized roles for Efcab6-like proteins in regulating centrosome function, microtubule stabilization, and/or axon extension. Localization to both the centrosome and later to the growth cone might be linking centrosome position to axon outgrowth, with Efcab6-related in the growth cone required later to promote further axon growth or guidance.

Of further note, *Ciona Efcab6-related* and *Dmbx* are neighboring genes, arrayed in a "head to head" manner and transcribed in opposite directions (Fig. 4H). A reporter construct spanning this putative shared *cis*-regulatory module and the translation start site of *Efcab6-related* was sufficient to drive expression in the ddNs (Fig. 4I). This fragment is overlapping with the *Dmbx* upstream *cis*-regulatory region that was originally used to drive reporter expression in the ddNs (Stolfi and Levine, 2011)(Fig. 4J). It also overlaps the smaller fragment used in this study to FACS-isolated the ddNs initially (Stolfi and Levine, 2011)(Fig. 4K), as well as the minimal *cis*-regulatory element that contains the Pax3/7 binding site required for *Dmbx* activation (Stolfi and Levine, 2011; Stolfi et al., 2011)(Fig. 4L). Since the minimal Pax3/7-binding module is roughly equidistant and 5' to both *Dmbx* and *Efcab6-related* (2.1 kb and 1.9 kb respectively, Fig. 4H), these two genes likely share a common regulatory element for ddN-specific expression. Given that Dmbx itself is a transcription factor that appears to inhibit proliferation and promote mitotic exit (Stolfi et al., 2011; Wong et al., 2015), this shared *cis*-regulatory element might be essential for coordination of genetically linked, but mechanistically distinct specification and morphogenetic processes in the ddNs.

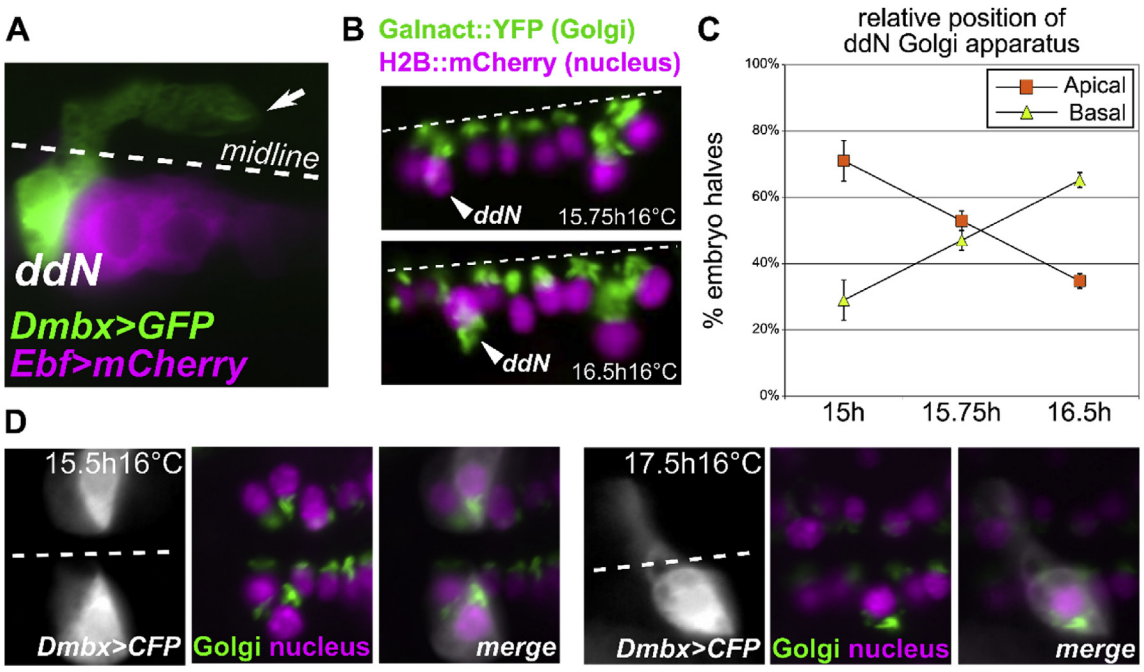

Fig. 5. Intracellular polarity dynamics in ddNs during contralateral axon outgrowth. **A)** MG cells labeled with *Ebf > Unc-76::mCherry* and ddN labeled with *Dmbx > Unc-76::GFP,* on one side of mosaic transgenic embryo. Arrow indicated ddN axon growth cone extending posteriorly. **B)** A9.30 lineage cell Golgi apparatuses labeled by *Fgf8/17/18 > Galnact::YFP* (Stolfi et al., 2015a) and nuclei labeled by *Fgf8/17/18 > H2B::mCherry* (Gline et al., 2009) showing intracellular polarity inversion in ddN between 15.75 and 16.5 h post-fertilization at 16 °C. **C)** Plot showing inversion of Golgi apparatus position in the ddNs, showing a shift from a more medial, apical position to a more lateral, basal position relative to cell nuclei. Each time point was analyzed in three independent replicates. In each replicate, $31 < n < 100$. Full data set contained in Supplemental Table 4. **D)** Three-color labeling showing Golgi apparatuses, nuclei, and cell body before (15.5 h, left panels) and after (17.5 h, right panels) inversion of polarity and axon extension across the midline (dashed lines).

The ddN-specific expression of known centrosome-enriched microtubule stabilizing proteins Nckap5 and Saxo, and the previously unrecognized centrosome marker Efcab6-related identified in this study, is interesting given the cellular processes that appear to underlie the unique contralateral axon projection of the ddNs. The ddN axon begins as an initial outgrowth that is oriented towards the neural tube lumen, extending across the midline (Fig. 5A). This is immediately preceded by a precisely timed, 180° re-orientation of the intracellular polarity of the cell, as visualized by the position of the Golgi apparatus, starting from an apical position apposing the neural tube lumen to a basal position near the neural tube basal lamina (Fig. 5B–D, Supplemental Table 4). In all other MG neurons, the Golgi apparatus remain on the apical side (lumen), and the direction of axon outgrowth is instead oriented away from the midline, resulting in an ipsilateral axon trajectory. A similar positioning of the Golgi apparatus on the opposite side of the nucleus relative to the site of axon extension was previously documented in migrating *Ciona* Bipolar Tail Neurons (BTNs), in which a precisely timed, 180° re-orientation of Golgi apparatus position also correlates with the direction of axon extension from an initially anterior orientation to a posterior one (Stolfi et al., 2015a). In these cases, the position of the Golgi apparatus is marker for centrosome position, which are tightly linked in vertebrate cells (Sütterlin and Colanzi, 2010) and in *Ciona* (Fig. 4E).

The relationship between centrosome/Golgi apparatus position and site of axonogenesis has been subject to long-running debates. Studies on cells *in vitro* suggested that the centrosome is positioned proximal to the site of axonogenesis (de Anda et al., 2005). However, more recent evidence suggests that *in vivo,* and depending on neuron type, centrosome position does not determine axon outgrowth and can even be *distal* to the site of axonogenesis (i.e. on the opposite side of the nucleus)(de Anda et al., 2010; Distel et al., 2010; Stolfi et al., 2015a; Zolessi et al., 2006). Since centrosome repositioning has been shown to depend on microtubule stabilization (Pitaval et al., 2017) the repositioning of ddN centrosomes that we observe might be effected in part by microtubule stabilization, driven by ddN-specific upregulation of *Saxo* and/or *Nckap5* (see follow up experiments below). *Saxo* transcripts were also detected in migrating BTNs by ISH (Fig. 4A), and by single-cell RNAseq analysis (Horie et al., 2018a), hinting at the possible involvement of Saxo in centrosome repositioning in BTNs too.

3.4. ddNs upregulate the axon guidance cue Netrin1

We found that the major axon guidance molecule-coding gene *Netrin1* (*KH.C12.72,* LogFC = 1.3)(Boyer and Gupton, 2018) is enriched in the ddN. We confirmed, by ISH, *Netrin1* expression specifically in the ddNs, among MG neurons (Fig. 6A,B). *Netrin1* is also highly expressed in the notochord (Hotta et al., 2000, 2007b), as is another axon guidance molecule, *Sema3a* (Kugler et al., 2008), supporting also a potential role of the notochord in guiding MG axons into the tail. Although Netrin was long thought to be exclusively a long-range cue (Kennedy et al., 1994; Serafini et al., 1994), tissue-specific targeting of *Netrin1* in the vertebrate hindbrain and spinal cord recently revealed that the role of netrin1 protein in guiding midline crossing is consistent with its function as a short-range cue. More specifically, netrin1 from the floorplate of the developing hindbrain is dispensable for midline crossing (Dominici et al., 2017; Yamauchi et al., 2017), which is mostly regulated by netrin1 distributed along the axon path and derived from ventricular zone progenitor progenitors instead. In the spinal cord, netrin from both sources act synergistically as short- and long-range cues to guide midline crossing (Dominici et al., 2017; Moreno-Bravo et al., 2019; Varadarajan et al., 2017; Wu et al., 2019). Furthermore, UNC-6/netrin in *C. elegans* is instructive for neuronal polarization and defines the site of axonogenesis (Adler et al., 2006). These short-range functions might explain the potential of ddN-deposited Netrin1 to specify the nascent axon medially and to serve as a short-range cue to drive axon extension towards the neural tube lumen and across the midline.

We also detected enrichment of transcripts from a gene encoding a relatively short, cysteine-rich predicted extracellular protein whose closest BLAST hits were the N-terminal heparin-binding and collagen-

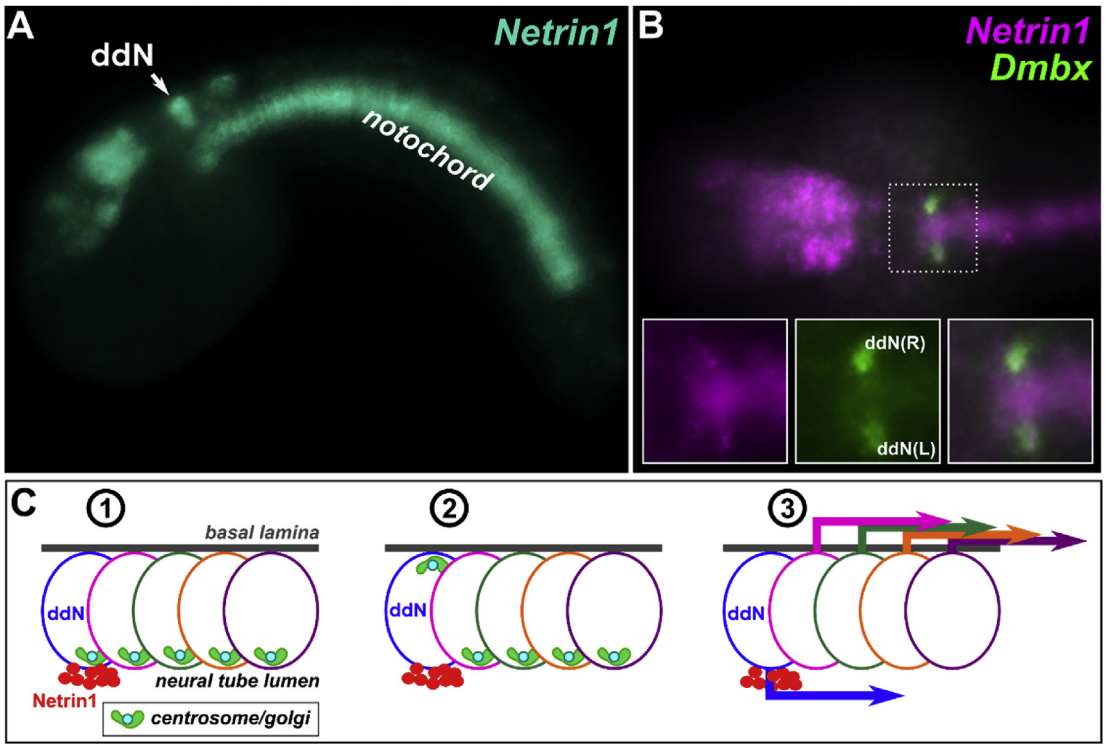

Fig. 6. Netrin1 expressed by ddNs and model for autocrine mechanism of ddN polarization. **A)** *In situ* hybridization of axon guidance cue-encoding *Netrin1,* showing expression in ddN (arrow) and notochord. **C)** Two-color *in situ* hybridization showing co-expression of *Netrin1* (magenta) and known ddN marker *Dmbx* (green). **D)** Cartoon diagram describing proposed model for an *intrinsic* program for ddN polarization, based on autocrine deposition of Netrin1. Briefly: 1) MG neural precursors on one side of the embryo depicted with their basal side pointing laterally, attached to the basal lamina of the neural tube, and their apical side (marked by centrosome and Golgi apparatus) pointing medially, exposed to the lumen of the neural tube. 2) the ddN expresses and apically secretes Netrin1, inverting its own polarity relative to other MG cells. 3) The ddN axon subsequently grows medially, away from basal lamina and towards the midline, eventually crossing the midline. All other neurons extend their axons laterally along the basal lamina of the neural tube.

binding domains of Fibronectin-like proteins from various organisms (see Supplemental Sequences). We termed this gene Fibronectin-related (Fn-related, KH.C2.667, LogFC = 1.7). However, expression of Fn-related was detected by ISH in the sister cell of the ddN, A12.240, and its progeny, but not in the ddN itself (Supplemental Fig. 7). Fn-related thus may have been a false-positive in our profiling, due to contamination by A12.240 or A12.240-like cells.

Among other poorly studied genes or genes without any obvious or specific function in establishing ddN-specific traits that were confirmed by ISH were *Fam167a* (*KH.C2.629,* LogFC = 3.1), *Calmodulin1-related (KH.C8.573,* LogFC = 2.3) and *Mitochondrial pyruvate carrier* (*KH.C1.85,* LogFC = 1.3)(Supplemental Figs. 8A–C). Additionally, we could not detect with any certainty the expression of two candidate genes in the ddNs by ISH, *Myosin10* and *Fibrillin* (Supplemental Figs. 8D and E). These negative results may have been due to poor probe design, which were prepared from short synthetic sequences (~500 bp). However, they also represent potentially false positives in the differential expression dataset, suggesting caution in interpreting such analysis devoid of any confirmatory ISH data.

3.5. Insights into ddN effector gene functions

To test the potential functions of certain ddN-specific effector genes, we used tissue-specific CRISPR/Cas9 (Stolfi et al., 2014) to knock them out in F0 embryos. First, we tested the function of *Efcab6-related,* since this gene family has been largely unstudied. We validated a single-chain guide RNA (sgRNA) that appeared to cut *Efcab6-related* most efficiently (*Efcab6r.167,* see **Supplemental Sequences**), as evidenced by short indels *in vivo* and elimination of *Ebf > Efcab6-related::GFP* expression in a lineage-specific manner (Supplemental Fig. 1). Using *Foxa.a>Cas9* to perform CRISPR/Cas9-mediated knockouts specifically in the vegetal lineages, from where the ddNs arise (Cole and Meinertzhagen, 2004), we assayed the effect of knocking out *Efcab6-related* on ddN development. Using *Dmbx > GFP* to visualize ddN axon outgrowth at the late tailbud stage (Stage 25, 12hpf/22 °C), we found that targeting *Efcab6-related* resulted in 45 of 100 (45%) ddNs with no clearly visible axon outgrowth (Fig. 7A,B). In control embryos (co-electroporated with *Cesa4.1*sgRNA vector instead, see **Materials and methods**), only 22 of 100 (22%) ddNs did not have a visible axon extending at this stage (Fig. 7A,B). We repeated this experiment, and found that *Efcab6-related* CRISPR resulted in 45 of 83 embryos with no visible axon (54%), compared to only 24 of 75 embryos in the control condition (32%) (Fig. 7B). We also quantified the lengths of randomly selected ddN axons from *Efcab6-related* and control animals, showing that embryos in the *Efcab6-related* CRISPR condition had a statistically significant (p = 0.039) reduction in axon length (Fig. 7C). Taken together, these results suggest that Efcab6-related is an important effector for axon outgrowth in the ddNs.

To test the potential role of Netrin1 as an intrinsic but *extracellular* positional cue that is required for ddN polarized axon outgrowth in an autocrine manner, we also used CRISPR/Cas9-mediated mutagenesis, but used instead *Fgf8/17/18 > Cas9* in order to carry out the *Netrin1* knockout specifically in the A9.30 lineage and not in other lineages expressing this gene (Fig. 7D). In one replicate, this resulted in only 42 of 97 (43%) ddNs with axons clearly projecting across the midline at 12 hpf/21 °C, compared to 27 of 43 (63%) in the control (co-electroporated with "Control" sgRNA vector instead). We repeated this, and in our second replicate we obtained only 14 of 65 (21%) ddNs visibly projecting across the midline in Netrin1 CRISPR, compared to only 45 of 71 (63%) in the control. Both replicates were scored blindly (Fig. 7D,E).

To test our model that Netrin1 may be an intrinsic cue deposited by the ddN to polarize itself, we assayed Golgi apparatus position in Netrin1 CRISPR mutants (Fig. 7F). In the control condition, we observed 51 of 77 (66%) embryos had at least one ddN with inverted Golgi position at

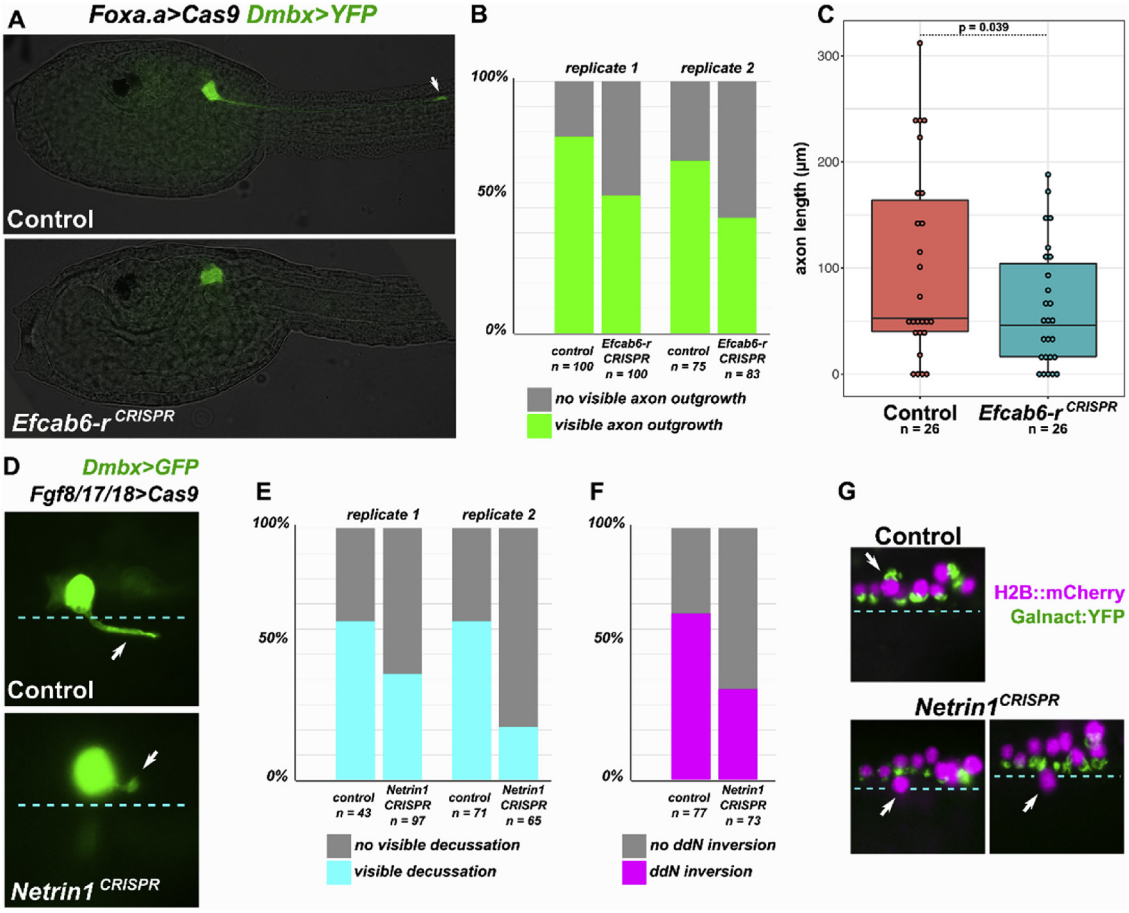

Fig. 7. CRISPR/Cas9-mediated knockout of ddN effectors Efcab6-related and Netrin1. **A)** A-line-specific knockout of *Efcab6-related* using *Foxa.a>Cas9* co-electroporated *U6>Efcab6-r.157* and *Dmbx > Unc-76::YFP* to visualize ddN axons. Top panel: "Control" condition performed side-by-side with *Efcab6-related* knockout, using instead 50 µg of *U6>Cesa4.1*. Axon growth cone indicated by arrow. **B)** Scoring percentage of embryos with visible axon growth in two biological replicates of the conditions depicted in (A). **C)** Plot of axon lengths measured in 26 embryos randomly selected from "Control" and *Efcab6-r* CRISPR conditions each. Statistical significance ($p = 0.039$) determined by one-tailed type 3 T-test. **D)** Knocking out *Netrin1* in A9.30 lineage using *Fgf8/17/18 > Cas9* co-electroporated with *U6>Netrin1.364* and *Dmbx > Unc-76::GFP*. Top panel: the control condition using *U6>Control* instead. Midlines indicated by dashed blue line. Nascent ddN axons indicated by arrows. **E)** Scoring percentage of embryos with visible axon decussation in two biological replicates of "Control" and *Netrin1* CRISPR conditions. **F)** Scoring percentage of embryos with visible ddN polarity inversion (visualized by H2B:mCherry to label nuclei and Galnact::YFP to label Golgi apparatus) in "Control" and *Netrin1* CRISPR conditions. **G)** Representative "Control" embryo showing inverted polarity of ddN (arrow) at 12 h/20 °C. Bottom panels: two instances of ddN nucleus translocation across the midline seen in *Netrin1* CRISPR embryos. Dashed lines indicate midline.

12hpf/20 °C, but in Netrin1 CRISPR, only 26 of 73 (36%) embryos did. These numbers are inversely correlated with the Golgi positions scored in wild-type embryos at the equivalent stage (16.5 hpf/16 °C, Fig. 5C). In at least two CRISPR mutant embryos, a ddN was observed to translocate its nucleus towards the midline, instead of away from the midline, a highly unusual phenotype that we have never observed before (Fig. 7G). This may reflect a non-cell-autonomous attractive effect of Netrin1 secreted from the ddN in the non-electroporated half of these embryos (thus also unlabeled by the fluorescent reporters), though a more careful investigation will be needed to parse cell-autonomous versus non-cell-autonomous effects of lineage-specific Netrin1 knockouts. Nonetheless, these data suggest that Netrin1, expressed by the ddN itself, is key to its characteristic polarization and subsequent axon outgrowth towards and across the midline.

4. Conclusions

Here we have used molecular perturbations, embryo dissociation, and FACS to isolate specific neuronal progenitors in the developing *Ciona* MG, and compared their transcriptomes by microarray. Specifically, we have compared ddN and MGIN2 neurons, which are predicted by the connectome to serve as major conduits for various sensory modalities to modulate the larva's swimming and escape response behaviors. Our transcriptome profiling points to possible effectors of ddN/MGIN2-specific electrophysiological properties (e.g. Scna.a, Kcna.a), morphology (e.g. Saxo, Nckap5, Efcab6-related, Pcdh.e), and functional connectivity (e.g. Chrnb, Gabrd, Grin). These now comprise an attractive set of targets for tissue-specific CRISPR/Cas9 somatic knockouts (Gandhi et al., 2017), in future functional studies of the gene regulatory networks regulating neurodevelopmental processes in the *Ciona* larva. We show that CRISPR/Cas9-mediated knockout of *Efcab6-related* and *Netrin1* produce ddN axon outgrowth defects consistent with the predicted involvement of these genes in ddN polarization and extension across the midline. Given the polarity defects observed in *Netrin1* CRISPR embryos, we predict that Netrin1 acts upstream of axon specification to polarize the ddNs 180° relative to neighboring, non-Netrin1-expressing cells. Given the different phenotype observed in *Efcab6-related* CRISPR embryos, in which ddNs more often failed to grow an axon or had shorter axons, we predict that Efcab6-related instead effects axon growth, possibly through its physical interaction with the centrosome and/or growth cone.

Our results suggest that both intracellular and extracellular effectors (e.g. Efcab6-related and Netrin1, respectively) are part of the same

intrinsic program that is deployed largely through ddN-specific transcriptional activation, blurring the line between fully extrinsic or intrinsic modes of neuronal polarization or axon guidance.

Acknowledgments

We thank Florian Razy-Krajka for discussions and feedback on data analysis and interpretations, and for key assistance with experiments. We thank Ellen LeMosy, William Smith, and Matthew Kourakis for insightful feedback and suggestions on the manuscript. We thank Nicole Kaplan and Lionel Christiaen for the Cesa4.1 sgRNA. We would like to acknowledge Efcab6 expression data provided by the JAX KOMP Phenotyping Center supported by NIH award U54HG006332. We thank the constant support of Michael Levine and Lionel Christiaen. This work was funded by NIH R00 award HD084814 to A.S., an NSF Graduate Research Fellowship to C.J.J., and a PURA award to J.O. from Georgia Tech.

Appendix A. Supplementary data

Supplementary data to this article can be found online at https://doi.org/10.1016/j.ydbio.2019.10.012.

References

Abitua, P.B., Wagner, E., Navarrete, I.A., Levine, M., 2012. Identification of a rudimentary neural crest in a non-vertebrate chordate. Nature 492, 104.
Adler, C.E., Fetter, R.D., Bargmann, C.I., 2006. UNC-6/Netrin induces neuronal asymmetry and defines the site of axon formation. Nat. Neurosci. 9, 511.
Baker, B.S., Taylor, B.J., Hall, J.C., 2001. Are complex behaviors specified by dedicated regulatory genes? Reasoning from Drosophila. Cell 105, 13–24.
Bargmann, C.I., 1993. Genetic and cellular analysis of behavior in C. elegans. Annu. Rev. Neurosci. 16, 47–71.
Beh, J., Shi, W., Levine, M., Davidson, B., Christiaen, L., 2007. FoxF is essential for FGF-induced migration of heart progenitor cells in the ascidian Ciona intestinalis. Development 134, 3297–3305.
Bolstad, B.M., Irizarry, R.A., Åstrand, M., Speed, T.P., 2003. A comparison of normalization methods for high density oligonucleotide array data based on variance and bias. Bioinformatics 19, 185–193.
Boyer, N.P., Gupton, S.L., 2018. Revisiting Netrin-1: one who guides (axons). Front. Cell. Neurosci. 12, 221.
Branicky, R., Miyazaki, H., Strange, K., Schafer, W.R., 2014. The voltage-gated anion channels encoded by clh-3 regulate egg laying in C. elegans by modulating motor neuron excitability. J. Neurosci. 34, 764–775.
Brown, E., Nishino, A., Bone, Q., Meinertzhagen, I., Okamura, Y., 2005. GABAergic synaptic transmission modulates swimming in the ascidian larva. Eur. J. Neurosci. 22, 2541–2548.
Canet-Avilés, R.M., Wilson, M.A., Miller, D.W., Ahmad, R., McLendon, C., Bandyopadhyay, S., Baptista, M.J., Ringe, D., Petsko, G.A., Cookson, M.R., 2004. The Parkinson's disease protein DJ-1 is neuroprotective due to cysteine-sulfinic acid-driven mitochondrial localization. Proc. Natl. Acad. Sci. 101, 9103–9108.
Cao, C., Lemaire, L.A., Wang, W., Yoon, P.H., Choi, Y.A., Parsons, L.R., Matese, J.C., Wang, W., Levine, M., Chen, K., 2019. Comprehensive single-cell transcriptome lineages of a proto-vertebrate. Nature 571, 349–354.
Chalfie, M., Sulston, J., White, J., Southgate, E., Thomson, J., Brenner, S., 1985. The neural circuit for touch sensitivity in Caenorhabditis elegans. J. Neurosci. 5, 956–964.
Christiaen, L., Davidson, B., Kawashima, T., Powell, W., Nolla, H., Vranizan, K., Levine, M., 2008. The transcription/migration interface in heart precursors of Ciona intestinalis. Science 320, 1349–1352.
Christiaen, L., Wagner, E., Shi, W., Levine, M., 2009a. Electroporation of transgenic DNAs in the sea squirt Ciona. Cold Spring Harb. Protoc. 2009 pdb. prot5345.
Christiaen, L., Wagner, E., Shi, W., Levine, M., 2009b. Isolation of sea squirt (Ciona) gametes, fertilization, dechorionation, and development. Cold Spring Harb. Protoc. 2009 pdb. prot5344.
Cole, A.G., Meinertzhagen, I.A., 2004. The central nervous system of the ascidian larva: mitotic history of cells forming the neural tube in late embryonic Ciona intestinalis. Dev. Biol. 271, 239–262.
Dacheux, D., Roger, B., Bosc, C., Landrein, N., Roche, E., Chansel, L., Trian, T., Andrieux, A., Papaxanthos-Roche, A., Marthan, R., 2015. Human FAM154A (SAXO1) is a microtubule-stabilizing protein specific to cilia and related structures. J. Cell Sci. 128, 1294–1307.
de Anda, F.C., Meletis, K., Ge, X., Rei, D., Tsai, L.-H., 2010. Centrosome motility is essential for initial axon formation in the neocortex. J. Neurosci. 30, 10391–10406.
de Anda, F.C., Pollarolo, G., Da Silva, J.S., Camoletto, P.G., Feiguin, F., Dotti, C.G., 2005. Centrosome localization determines neuronal polarity. Nature 436, 704–708.
Delsuc, F., Brinkmann, H., Chourrout, D., Philippe, H., 2006. Tunicates and not cephalochordates are the closest living relatives of vertebrates. Nature 439.
Di Gregorio, A., Corbo, J.C., Levine, M., 2001. The regulation of forkhead/HNF-3β expression in the Ciona embryo. Dev. Biol. 229, 31–43.
Distel, M., Hocking, J.C., Volkmann, K., Köster, R.W., 2010. The centrosome neither persistently leads migration nor determines the site of axonogenesis in migrating neurons in vivo. J. Cell Biol. 191, 875–890.
Dominici, C., Moreno-Bravo, J.A., Puiggros, S.R., Rappeneau, Q., Rama, N., Vieugue, P., Bernet, A., Mehlen, P., Chédotal, A., 2017. Floor-plate-derived netrin-1 is dispensable for commissural axon guidance. Nature 545, 350.
Dynes, J.L., Ngai, J., 1998. Pathfinding of olfactory neuron axons to stereotyped glomerular targets revealed by dynamic imaging in living zebrafish embryos. Neuron 20, 1081–1091.
Gandhi, S., Haeussler, M., Razy-Krajka, F., Christiaen, L., Stolfi, A., 2017. Evaluation and rational design of guide RNAs for efficient CRISPR/Cas9-mediated mutagenesis in Ciona. Dev. Biol. 425, 8–20.
Gandhi, S., Razy-Krajka, F., Christiaen, L., Stolfi, A., 2018. CRISPR Knockouts in Ciona Embryos, Transgenic Ascidians. Springer, pp. 141–152.
Garrido, J.J., Giraud, P., Carlier, E., Fernandes, F., Moussif, A., Fache, M.-P., Debanne, D., Dargent, B., 2003. A targeting motif involved in sodium channel clustering at the axonal initial segment. Science 300, 2091–2094.
Gline, S.E., Kuo, D.-H., Stolfi, A., Weisblat, D.A., 2009. High resolution cell lineage tracing reveals developmental variability in leech. Dev. Dynam. 238, 3139–3151.
Haeussler, M., Schönig, K., Eckert, H., Eschstruth, A., Mianné, J., Renaud, J.-B., Schneider-Maunoury, S., Shkumatava, A., Teboul, L., Kent, J., 2016. Evaluation of off-target and on-target scoring algorithms and integration into the guide RNA selection tool CRISPOR. Genome Biol. 17, 148.
Hill, A.S., Nishino, A., Nakajo, K., Zhang, G., Fineman, J.R., Selzer, M.E., Okamura, Y., Cooper, E.C., 2008. Ion channel clustering at the axon initial segment and node of ranvier evolved sequentially in early chordates. PLoS Genet. 4, e1000317.
Horie, R., Hazbun, A., Chen, K., Cao, C., Levine, M., Horie, T., 2018a. Shared evolutionary origin of vertebrate neural crest and cranial placodes. Nature 560, 228.
Horie, T., Horie, R., Chen, K., Cao, C., Nakagawa, M., Kusakabe, T.G., Satoh, N., Sasakura, Y., Levine, M., 2018b. Regulatory cocktail for dopaminergic neurons in a protovertebrate identified by whole-embryo single-cell transcriptomics. Genes Dev. 32, 1297–1302.
Horie, T., Kusakabe, T., Tsuda, M., 2008. Glutamatergic networks in the Ciona intestinalis larva. J. Comp. Neurol. 508, 249–263.
Hotta, K., Mitsuhara, K., Takahashi, H., Inaba, K., Oka, K., Gojobori, T., Ikeo, K., 2007a. A web-based interactive developmental table for the ascidian Ciona intestinalis, including 3D real-image embryo reconstructions: I. From fertilized egg to hatching larva. Dev. Dynam. 236, 1790–1805.
Hotta, K., Takahashi, H., Asakura, T., Saitoh, B., Takatori, N., Satou, Y., Satoh, N., 2000. Characterization of Brachyury-downstream notochord genes in the Ciona intestinalis embryo. Dev. Biol. 224, 69–80.
Hotta, K., Yamada, S., Ueno, N., Satoh, N., Takahashi, H., 2007b. Brachyury-downstream notochord genes and convergent extension in Ciona intestinalis embryos. Dev. Growth Differ. 49, 373–382.
Hsiau, T., Conant, D., Rossi, N., Maures, T., Waite, K., Yang, J., Joshi, S., Kelso, R., Holden, K., Enzmann, B.L., Stoner, R., 2019. Inference of CRISPR Edits from Sanger Trace Data bioRxiv, 251082.
Ikuta, T., Saiga, H., 2007. Dynamic change in the expression of developmental genes in the ascidian central nervous system: revisit to the tripartite model and the origin of the midbrain–hindbrain boundary region. Dev. Biol. 312, 631–643.
Imai, J.H., Meinertzhagen, I.A., 2007. Neurons of the ascidian larval nervous system in Ciona intestinalis: II. Peripheral nervous system. J. Comp. Neurol. 501, 335–352.
Imai, K.S., Hino, K., Yagi, K., Satoh, N., Satou, Y., 2004. Gene expression profiles of transcription factors and signaling molecules in the ascidian embryo: towards a comprehensive understanding of gene networks. Development 131, 4047–4058.
Imai, K.S., Stolfi, A., Levine, M., Satou, Y., 2009. Gene regulatory networks underlying the compartmentalization of the Ciona central nervous system. Development 136, 285–293.
Ito, D., Bettencourt-Dias, M., 2018. Centrosome remodelling in evolution. Cells 7, 71.
Jang, H., Kim, K., Neal, S.J., Macosko, E., Kim, D., Butcher, R.A., Zeiger, D.M., Bargmann, C.I., Sengupta, P., 2012. Neuromodulatory state and sex specify alternative behaviors through antagonistic synaptic pathways in C. elegans. Neuron 75, 585–592.
Jiang, D., Tresser, J.W., Horie, T., Tsuda, M., Smith, W.C., 2005. Pigmentation in the sensory organs of the ascidian larva is essential for normal behavior. J. Exp. Biol. 208, 433–438.
Katoh, K., Rozewicki, J., Yamada, K.D., 2017. MAFFT online service: multiple sequence alignment, interactive sequence choice and visualization. Briefings Bioinf. 20, 1160–1166.
Katsuyama, Y., Okada, T., Matsumoto, J., Ohtsuka, Y., Terashima, T., Okamura, Y., 2005. Early specification of ascidian larval motor neurons. Dev. Biol. 278, 310–322.
Keeler, A.B., Molumby, M.J., Weiner, J.A., 2015. Protocadherins branch out: multiple roles in dendrite development. Cell Adhes. Migrat. 9, 214–226.
Kennedy, T.E., Serafini, T., de la Torre, J., Tessier-Lavigne, M., 1994. Netrins are diffusible chemotropic factors for commissural axons in the embryonic spinal cord. Cell 78, 425–435.
Kim, B., Emmons, S.W., 2017. Multiple conserved cell adhesion protein interactions mediate neural wiring of a sensory circuit in C. elegans. Elife 6, e29257.
Kole, M.H., Ilschner, S.U., Kampa, B.M., Williams, S.R., Ruben, P.C., Stuart, G.J., 2008. Action potential generation requires a high sodium channel density in the axon initial segment. Nat. Neurosci. 11, 178.
Kourakis, M.J., Borba, C., Zhang, A., Newman-Smith, E., Salas, P., Manjunath, B., Smith, W.C., 2019. Parallel visual circuitry in a basal chordate. eLife 8, e44753.
Kugler, J.E., Passamaneck, Y.J., Feldman, T.G., Beh, J., Regnier, T.W., Di Gregorio, A., 2008. Evolutionary conservation of vertebrate notochord genes in the ascidian Ciona intestinalis. Genesis 46, 697–710.

Lemaillet, G., Walker, B., Lambert, S., 2003. Identification of a conserved ankyrin-binding motif in the family of sodium channel α subunits. J. Biol. Chem. 278, 27333–27339.
Luo, L., Callaway, E.M., Svoboda, K., 2008. Genetic dissection of neural circuits. Neuron 57, 634–660.
Manoli, D.S., Meissner, G.W., Baker, B.S., 2006. Blueprints for behavior: genetic specification of neural circuitry for innate behaviors. Trends Neurosci. 29, 444–451.
Moreno-Bravo, J.A., Puiggros, S.R., Mehlen, P., Chédotal, A., 2019. Synergistic activity of floor-plate-and ventricular-zone-derived Netrin-1 in spinal cord commissural axon guidance. Neuron 101, 625–634 e623.
Moret, F., Christiaen, L., Deyts, C., Blin, M., Joly, J.S., Vernier, P., 2005. The dopamine-synthesizing cells in the swimming larva of the tunicate Ciona intestinalis are located only in the hypothalamus-related domain of the sensory vesicle. Eur. J. Neurosci. 21.
Mori, Y., Inoue, Y., Tanaka, S., Doda, S., Yamanaka, S., Fukuchi, H., Terada, Y., 2015a. Cep169, a novel microtubule plus-end-tracking centrosomal protein, binds to CDK5RAP2 and regulates microtubule stability. PLoS One 10, e0140968.
Mori, Y., Taniyama, Y., Tanaka, S., Fukuchi, H., Terada, Y., 2015b. Microtubule-bundling activity of the centrosomal protein, Cep169, and its binding to microtubules. Biochem. Biophys. Res. Commun. 467, 754–759.
Nakashima, K., Yamada, L., Satou, Y., Azuma, J.-i., Satoh, N., 2004. The evolutionary origin of animal cellulose synthase. Dev. Gene. Evol. 214, 81–88.
Navarrete, I.A., Levine, M., 2016. Nodal and FGF coordinate ascidian neural tube morphogenesis. Development 143, 4665–4675.
Nicol, D., Meinertzhagen, I., 1988a. Development of the central nervous system of the larva of the ascidian, Ciona intestinalis L: I. The early lineages of the neural plate. Dev. Biol. 130, 721–736.
Nicol, D., Meinertzhagen, I., 1988b. Development of the central nervous system of the larva of the ascidian, Ciona intestinalis L: II. Neural plate morphogenesis and cell lineages during neurulation. Dev. Biol. 130, 737–766.
Niki, T., Takahashi-Niki, K., Taira, T., Iguchi-Ariga, S.M., Ariga, H., 2003. DJBP: a novel DJ-1-binding protein, negatively regulates the androgen receptor by recruiting Histone deacetylase complex, and DJ-1 antagonizes this inhibition by abrogation of this complex. Mol. Cancer Res. 1, 247–261.
Nishino, A., 2018. Morphology and Physiology of the Ascidian Nervous Systems and the Effectors, Transgenic Ascidians. Springer, pp. 179–196.
Nishino, A., Okamura, Y., 2018. Evolutionary history of voltage-gated sodium channels. In: Chahine, M. (Ed.), Voltage-gated Sodium Channels: Structure, Function and Channelopathies. Springer International Publishing, Cham, pp. 3–32.
Nishino, A., Okamura, Y., Piscopo, S., Brown, E.R., 2010. A glycine receptor is involved in the organization of swimming movements in an invertebrate chordate. BMC Neurosci. 11, 6.
Nishitsuji, K., Horie, T., Ichinose, A., Sasakura, Y., Yasuo, H., Kusakabe, T.G., 2012. Cell lineage and cis-regulation for a unique GABAergic/glycinergic neuron type in the larval nerve cord of the ascidian Ciona intestinalis. Dev. Growth Differ. 54, 177–186.
O'Brien, K.P., Remm, M., Sonnhammer, E.L.L., 2005. Inparanoid: a comprehensive database of eukaryotic orthologs. Nucleic Acids Res. 33, D476–D480.
Okamura, Y., Nishino, A., Murata, Y., Nakajo, K., Iwasaki, H., Ohtsuka, Y., Tanaka-Kunishima, M., Takahashi, N., Hara, Y., Yoshida, T., 2005. Comprehensive analysis of the ascidian genome reveals novel insights into the molecular evolution of ion channel genes. Physiol. Genom. 22, 269–282.
Ono, F., Katsuyama, Y., Nakajo, K., Okamura, Y., 1999. Subfamily-specific posttranscriptional mechanism underlies K+ channel expression in a developing neuronal blastomere. J. Neurosci. 19, 6874–6886.
Pennati, R., Ficetola, G.F., Brunetti, R., Caicci, F., Gasparini, F., Griggio, F., Sato, A., Stach, T., Kaul-Strehlow, S., Gissi, C., Manni, L., 2015. Morphological differences between larvae of the Ciona intestinalis species complex: hints for a valid taxonomic definition of distinct species. PLoS One 10, e0122879.
Pitaval, A., Senger, F., Letort, G., Gidrol, X., Guyon, L., Sillibourne, J., Théry, M., 2017. Microtubule stabilization drives 3D centrosome migration to initiate primary ciliogenesis. J. Cell Biol. 216, 3713–3728.
Razy-Krajka, F., Brown, E.R., Horie, T., Callebert, J., Sasakura, Y., Joly, J.-S., Kusakabe, T.G., Vernier, P., 2012. Monoaminergic modulation of photoreception in ascidian: evidence for a proto-hypothalamo-retinal territory. BMC Biol. 10, 45.
Razy-Krajka, F., Lam, K., Wang, W., Stolfi, A., Joly, M., Bonneau, R., Christiaen, L., 2014. Collier/OLF/EBF-dependent transcriptional dynamics control pharyngeal muscle specification from primed cardiopharyngeal progenitors. Dev. Cell 29, 263–276.
Rudolf, J., Dondorp, D., Canon, L., Tieo, S., Chatzigeorgiou, M., 2019. Automated behavioural analysis reveals the basic behavioural repertoire of the urochordate Ciona intestinalis. Sci. Rep. 9, 2416.
Ryan, K., Lu, Z., Meinertzhagen, I.A., 2016. The CNS connectome of a tadpole larva of Ciona intestinalis (L.) highlights sidedness in the brain of a chordate sibling. Elife 5.
Ryan, K., Lu, Z., Meinertzhagen, I.A., 2017. Circuit homology between decussating pathways in the Ciona larval CNS and the vertebrate startle-response pathway. Curr. Biol. 27, 721–728.
Ryan, K., Lu, Z., Meinertzhagen, I.A., 2018. The peripheral nervous system of the ascidian tadpole larva: types of neurons and their synaptic networks. J. Comp. Neurol. 526, 583–608.
Ryan, K., Meinertzhagen, I.A., 2019. Neuronal identity: the neuron types of a simple chordate sibling, the tadpole larva of Ciona intestinalis. Curr. Opin. Neurobiol. 56, 47–60.
Salas, P., Vinaithirthan, V., Newman-Smith, E., Kourakis, M.J., Smith, W.C., 2018. Photoreceptor specialization and the visuomotor repertoire of the primitive chordate Ciona. J. Exp. Biol. 221, jeb177972.
Satou, Y., Mineta, K., Ogasawara, M., Sasakura, Y., Shoguchi, E., Ueno, K., Yamada, L., Matsumoto, J., Wasserscheid, J., Dewar, K., 2008. Improved genome assembly and evidence-based global gene model set for the chordate Ciona intestinalis: new insight into intron and operon populations. Genome Biol. 9, R152.
Serafini, T., Kennedy, T.E., Gaiko, M.J., Mirzayan, C., Jessell, T.M., Tessier-Lavigne, M., 1994. The netrins define a family of axon outgrowth-promoting proteins homologous to C. elegans UNC-6. Cell 78, 409–424.
Sharma, S., Wang, W., Stolfi, A., 2019. Single-cell transcriptome profiling of the Ciona larval brain. Dev. Biol. 448, 226–236.
Smyth, G.K., 2004. Linear models and empirical bayes methods for assessing differential expression in microarray experiments. Stat. Appl. Genet. Mol. Biol. 3. Article3.
Sporns, O., Tononi, G., Kötter, R., 2005. The human connectome: a structural description of the human brain. PLoS Comput. Biol. 1, e42.
Stolfi, A., Gandhi, S., Salek, F., Christiaen, L., 2014. Tissue-specific genome editing in Ciona embryos by CRISPR/Cas9. Development 141, 4115–4120.
Stolfi, A., Levine, M., 2011. Neuronal subtype specification in the spinal cord of a protovertebrate. Development 138, 995–1004.
Stolfi, A., Ryan, K., Meinertzhagen, I.A., Christiaen, L., 2015a. Migratory neuronal progenitors arise from the neural plate borders in tunicates. Nature 527, 371.
Stolfi, A., Sasakura, Y., Chalopin, D., Satou, Y., Christiaen, L., Dantec, C., Endo, T., Naville, M., Nishida, H., Swalla, B.J., 2015b. Guidelines for the Nomenclature of Genetic Elements in Tunicate Genomes. Genesis.
Stolfi, A., Wagner, E., Taliaferro, J.M., Chou, S., Levine, M., 2011. Neural tube patterning by Ephrin, FGF and Notch signaling relays. Development 138, 5429–5439.
Sütterlin, C., Colanzi, A., 2010. The Golgi and the centrosome: building a functional partnership. J. Cell Biol. 188, 621–628.
Takamura, K., Minamida, N., Okabe, S., 2010. Neural map of the larval central nervous system in the ascidian Ciona intestinalis. Zool. Sci. 27, 191–203.
Thompson, A., Gribizis, A., Chen, C., Crair, M.C., 2017. Activity-dependent development of visual receptive fields. Curr. Opin. Neurobiol. 42, 136–143.
Tsuda, M., Sakurai, D., Goda, M., 2003. Direct evidence for the role of pigment cells in the brain of ascidian larvae by laser ablation. J. Exp. Biol. 206, 1409–1417.
Varadarajan, S.G., Kong, J.H., Phan, K.D., Kao, T.-J., Panaitof, S.C., Cardin, J., Eltzschig, H., Kania, A., Novitch, B.G., Butler, S.J., 2017. Netrin1 produced by neural progenitors, not floor plate cells, is required for axon guidance in the spinal cord. Neuron 94, 790–799 e793.
Wang, W., Racioppi, C., Gravez, B., Christiaen, L., 2018. Purification of Fluorescent Labeled Cells from Dissociated Ciona Embryos, Transgenic Ascidians. Springer, pp. 101–107.
Wang, X., Petrie, T.G., Liu, Y., Liu, J., Fujioka, H., Zhu, X., 2012. Parkinson's disease-associated DJ-1 mutations impair mitochondrial dynamics and cause mitochondrial dysfunction. J. Neurochem. 121, 830–839.
White, J., Southgate, E., Thomson, J., 1992. Mutations in the Caenorhabditis elegans unc–4 gene alter the synaptic input to ventral cord motor neurons. Nature 355, 838.
White, J.G., Southgate, E., Thomson, J.N., Brenner, S., 1986. The structure of the nervous system of the nematode Caenorhabditis elegans. Philos. Trans. R. Soc. Lond. B Biol. Sci. 314, 1–340.
Wong, L., Power, N., Miles, A., Tropepe, V., 2015. Mutual antagonism of the paired-type homeobox genes, vsx2 and dmbx1, regulates retinal progenitor cell cycle exit upstream of ccnd1 expression. Dev. Biol. 402, 216–228.
Wu, Z., Makihara, S., Yam, P.T., Teo, S., Renier, N., Balekoglu, N., Moreno-Bravo, J.A., Olsen, O., Chédotal, A., Charron, F., 2019. Long-range guidance of spinal commissural axons by Netrin1 and Sonic Hedgehog from midline floor plate cells. Neuron 101, 635–647 e634.
Yamamoto, D., Koganezawa, M., 2013. Genes and circuits of courtship behaviour in Drosophila males. Nat. Rev. Neurosci. 14, 681.
Yamauchi, K., Yamazaki, M., Abe, M., Sakimura, K., Lickert, H., Kawasaki, T., Murakami, F., Hirata, T., 2017. Netrin-1 derived from the ventricular zone, but not the floor plate, directs hindbrain commissural axons to the ventral midline. Sci. Rep. 7, 11992.
Zhang, L.I., Poo, M.-m., 2001. Electrical activity and development of neural circuits. Nat. Neurosci. 4, 1207.
Zolessi, F.R., Poggi, L., Wilkinson, C.J., Chien, C.-B., Harris, W.A., 2006. Polarization and orientation of retinal ganglion cells in vivo. Neural Dev. 1, 2.